

Carbon isotopic signature of coal-derived methane emissions to atmosphere: from coalification to alteration

Giulia Zazzeri¹, Dave Lowry¹, Rebecca E. Fisher¹, James L. France^{1,2}, Mathias Lanoisellé¹, Bryce F.J. Kelly⁴, Jaroslaw M. Necki³, Charlotte P. Iverach⁴, Elisa Ginty⁴, Mirosław Zimnoch³, Alina Jasek³ and Euan G. Nisbet¹.

¹Royal Holloway University of London, Egham Hill, Egham, Surrey TW20 0EX

²University of East Anglia, Norwich Research Park, Norwich, Norfolk NR4 7TJ

³AGH-University of Science and Technology, Al.Mickiewicza 30 Kraków, Poland

⁴Connected Waters Initiative Research Centre, UNSW Australia

Correspondence to: Dr Giulia Zazzeri (Giulia.Zazzeri.2011@live.rhul.ac.uk)

Prof Euan Nisbet (e.nisbet@es.rhul.ac.uk)

Abstract. Currently, the atmospheric methane burden is rising rapidly, but the extent to which shifts in coal production contribute to this rise is not known. Coalbed methane emissions into the atmosphere are poorly characterised, and this study provides representative $\delta^{13}\text{CCH}_4$ signatures of methane emissions from specific coalfields. Integrated methane emissions from both underground and opencast coal mines in the UK, Australia and Poland were sampled and isotopically characterised. Progression in coal rank and secondary biogenic production of methane due to incursion of water are suggested as the processes affecting the isotopic composition of coal-derived methane. An averaged value of -65 ‰ has been assigned to bituminous coal exploited in open cast mines and of -55 ‰ in deep mines, whereas values of -40 ‰ and -30 ‰ can be allocated to anthracite opencast and deep mines respectively. However, the isotopic signatures that are included in global atmospheric modelling of coal emissions should be region or nation specific, as greater detail is needed, given the wide global variation in coal type.

1 Introduction

Methane emissions from the energy sector have been driven in recent years by the impact of a shift from coal to natural gas, in the US and Europe, whereas in China coal production has increased in this century. Currently, the atmospheric methane burden is rising rapidly (Nisbet et al., 2014), but the extent to which shifts in coal production contribute to this rise is not known. Coalbed methane emissions into the atmosphere are poorly characterised, as they are dispersed over large areas and continue even after the mines' closure (IPCC, 2006). Methane is emitted in coal processing (crushing and pulverisation) and during the initial removal of the overburden; it can be diluted and emitted through ventilation shafts in underground coal mines, or directly emitted to atmosphere from open-cut coal mining, where releases may occur as a result of deterioration of the coal seam.

For the UN Framework Convention on Climate Change, national emissions are estimated by a "bottom-up" approach, based upon a general equation where the coal production data are multiplied by an emission factor that takes into account the mine's gassiness, which in turn is related to the depth of the mine and the coal rank (i.e. carbon content of coal) (U.S. EPA, 2013). These modelled estimates are often reported without an error assessment, and therefore the level of accuracy of the emissions is not known. "Top-down" assessment of methane

39 emissions can be made by chemical transport models constrained by atmospheric measurements (Bousquet et al.,
40 2006; Locatelli et al., 2013). However, this top-down approach provides the total amount of methane emissions
41 into the atmosphere, which has to be distributed among the different methane sources in order to quantify each
42 source contribution.

43 For methane emissions from fossil fuels (coal and natural gas), the source partitioning is mainly “bottom-up”,
44 based on energy use statistics and local inventories, which might be highly uncertain. Conversely, the “top-down”
45 study of the carbon isotopic composition of methane, which is indicative of the methane origin, provides a valuable
46 constraint on the budget appraisal, allowing different sources in a source mix to be distinguished and their
47 individual strength to be evaluated (Hein et al., 1997; Liptay et al., 1998; Lowry et al., 2001; Townsend-Small et
48 al., 2012).

49 Measurements of methane mole fractions can be complemented in atmospheric models by typical $\delta^{13}\text{CCH}_4$
50 signatures of the main methane sources in order to estimate global and regional methane emissions and assess
51 emissions scenarios throughout the past years (Fung et al., 1991; Miller, 2004; Whiticar and Schaefer, 2007;
52 Bousquet et al., 2006; Monteil et al., 2011; Mikaloff Fletcher et al., 2014). However, even though isotopic values
53 are fairly distinctive for specific methanogenic processes, the variety of production pathways and local
54 environmental conditions that discriminate the methane formation process leads to a wide range of $\delta^{13}\text{CCH}_4$
55 values. The global isotopic range for coal is very large, from -80 to -17 ‰ (Rice, 1993), but it can be narrowed
56 down when a specific basin is studied. While there are several studies of isotopic composition of methane
57 generated from coal in Australia, U.S.A. and China (Smith and Rigby, 1981; Dai et al., 1987; Rice et al., 1989;
58 Aravena et al., 2003; Flores et al., 2008; Papendik et al., 2011), there is a significant lack of information about the
59 isotopic characterisation of methane emissions from coal mines in Europe.

60 The purpose of this study was to determine links between $\delta^{13}\text{CCH}_4$ signatures and coal rank and mining setting,
61 and to provide representative ^{13}C signatures to be used in atmospheric models in order to produce more accurate
62 methane emission estimates for the coal exploitation sector.

63 **Process of coalification and parameters affecting the $\delta^{13}\text{C}$ signature of methane emissions**

64 The process of coalification involves both biochemical and geochemical reactions. The vegetal matter firstly
65 decays anaerobically under water; the simple molecules derived from initial decomposition (i.e. acetate, CO_2 , H_2 ,
66 NH_4^+ , HS^- , long chain fatty acids) are metabolised by fermentative archaea, which produce methane via two
67 methanogenic paths: acetoclastic reaction or CO_2 reduction (Whiticar, 1999). Different pathways lead to diverse
68 $\delta^{13}\text{CCH}_4$ isotopic signatures - methane from acetate is ^{13}C enriched relative to methane from CO_2 reduction,
69 ranging from -65 ‰ to -50 ‰ and -110 ‰ to -50 ‰ respectively (Levin et al., 1993; Waldron et al., 1998). With
70 increasing burial and temperatures, coal is subjected to thermal maturation, which implicates more geochemical
71 changes.

72 As coalification proceeds, the carbon content increases, accompanied by a relative depletion in volatile
73 compounds, such as hydrogen and oxygen, emitted in the form of water, methane, carbon dioxide and higher
74 hydrocarbons through decarboxylation and dehydration reactions (Stach and Murchison, 1982). At higher degrees
75 of coalification and temperature, the liquid hydrocarbons formed in previous stages are thermally cracked to
76 methane, increasing the amount of methane produced (Faiz and Hendry, 2006). Peat and brown coal represent the
77 first stage of the coalification process. The vertical pressure exerted by accumulating sediments converts peat into

78 lignite. The intensification of the pressure and heat results in the transition from lignite to bituminous coal, and
79 eventually to anthracite, the highest rank of coal (O'Keefe et al., 2013).

80 During peat and brown coal stages, primary biogenic methane is formed and it is mainly dissolved in water or
81 released during burial, as coal is not appropriately structured for gas retention (Kotarba and Rice, 2001). At more
82 mature stages, thermogenic methane is produced by thermal modification of sedimentary organic matter, which
83 occurs at great depths and intensive heat. Following the basin uplift, methane production can be triggered in the
84 shallower sediments by the meteoric water inflow into the coal (secondary biogenic gas) (Rice, 1993; Scott et al.,
85 1994).

86 The isotopic signature of the methane produced during the coalification process is controlled by the methane
87 origin pathway (Whiticar, 1996). Thermogenic methane is isotopically enriched in ^{13}C ($\delta^{13}\text{C} > -50\text{‰}$) compared
88 to biogenic methane, as methanogens preferentially use the lightest isotopes due to the lower bond energy (Rice,
89 1993). Intermediate isotopic compositions of methane might reflect a mixing between microbial and thermogenic
90 gases or secondary processes. Indeed, many controlling factors co-drive the fractionation process, and several
91 contentions about their leverage still persist in literature. Deines (1980) asserts that no significant trend is observed
92 in the isotopic signature of methane in relation to the degree of coalification. Conversely, Chung et al. (1979)
93 observed that the composition of the parent material does affect the isotopic composition of the methane
94 accumulated. While the link between isotopic composition and coal rank is not that straightforward, studies carried
95 out in different worldwide coal seams confirm a stronger relationship between coal bed gas composition and
96 depth. Rice (1993), using data from Australian, Chinese and German coal beds, shows that shallow coal beds tend
97 to contain relatively isotopically lighter methane when compared to those at greater depths. In the presence of
98 intrusions of meteoric water, secondary biogenic methane, isotopically lighter, can be generated and mixed with
99 the thermogenic gas previously produced. Colombo et al. (1966) documented a distinct depth correlation in the
100 Ruhr Basin coal in Germany, with methane becoming more ^{13}C -depleted towards the surface zone, independently
101 from coalification patterns. This tendency can be explained either by bacterial methanogenesis, or by secondary
102 processes such as absorption-desorption of methane. Also Scott (2002), in a study about coal seams in the Bowen
103 Basin, Australia, ascribes the progressive methane ^{13}C -enrichment with depth to the meteoritic recharge in the
104 shallowest seams, associated with a higher bacterial activity and a preferential stripping of ^{13}C - CH_4 by water flow.
105 The migration of methane from the primary zone as a consequence of local pressure release can affect the isotopic
106 composition, since $^{12}\text{CH}_4$ diffuses and desorbs more readily than $^{13}\text{CH}_4$ (Deines, 1980), but the fractionation effect
107 due to migration is less than 1 ‰ (Fuex, 1980). A much larger variation in the isotopic composition is associated
108 with different methanogenic pathways (variation of $\sim 30\text{‰}$) and thermal maturation stage (variation of $\sim 25\text{‰}$)
109 (Clayton, 1998). The measurement of Deuterium, coupled with $\delta^{13}\text{CCH}_4$ values, would help to distinguish the
110 pathways of secondary biogenic methane generation, acetoclastic reactions or CO_2 reduction (Faiz and Hendry,
111 2006), but such distinction is beyond the scope of this study.

112 Overall, the $\delta^{13}\text{C}$ values of methane from coal show an extremely wide range and understanding the processes
113 driving the methane isotopic composition needs to focus on the particular set of geological conditions in each
114 sedimentary basin.

115 Here we analyse the isotopic signatures of methane plumes emitted to atmosphere, from the dominant bituminous
116 and anthracite mines in Europe and Australia, of both deep and open cut type, to test the theory of isotopic change
117 due to coal rank.

118 2 Material and Methods

119 2.1 Coal basins investigated and type of coal exploited

120 2.1.1 English and Welsh coal mines

121 Coal-derived methane emissions in the UK are estimated at 66 Gg in 2013 (naei.defra.gov.uk), representing 0.4%
122 of global emissions from mining activity (US EPA, 2012). The major coalfields of England and Wales belong to
123 the same stage in the regional stratigraphy of northwest Europe (Westphalian Stage, Upper Carboniferous).
124 Mining has ceased in many areas. Of those remaining some are located in South Yorkshire (Hatfield and Maltby
125 collieries), where 50% of the coalfield's output came from the Barnsley seam, which includes soft coal overlaying
126 a semi-anthracitic coal and bituminous coal in the bottom portion.

127 The coal of the South Wales basin exhibits a well-defined regional progression in rank, which varies from highly
128 volatile bituminous coal in the south and east margin to anthracite in the north-west part, and the main coal-bearing
129 units reach 2.75 km in thickness toward the south-west of the coalfield (Alderton et al., 2004). The coal is now
130 preferentially extracted in opencast mines, as the extensive exploitation of the coal has left the accessible resources
131 within highly deformed structures (e.g. thrust overlaps, vertical faults) that cannot be worked by underground
132 mining methods (Frodsham and Gayer, 1999). Emissions from two deep mines, Unity and Aberpergwm, were
133 investigated, where mine shafts reach depths up to approximately 750 m ([http://www.wales-
134 underground.org.uk/pit/geology.shtml](http://www.wales-underground.org.uk/pit/geology.shtml)).

135 2.1.2 Upper Silesian Coal Basin in Poland

136 The Upper Silesian Coal Basin extends from Poland to the Czech Republic and is one of the largest coal basins
137 in Europe, with an area of ~7400 km² (Jureczka and Kotas, 1995), contributing 1.3% to global coal-derived
138 methane emissions (US EPA, 2012). Emissions from the Silesian Region of Poland are estimated to be in the
139 range of 450-1350 Gg annually (Patyńska, 2013). The upper Carboniferous coal-bearing strata of this region are
140 associated with gas deposits of both thermogenic and microbial origin, and the methane content and spatial
141 distribution are coal rank related (Kędzior, 2009) - i.e. the sorption capacity of coal in the basin is found to increase
142 with coal rank. Most of the methane generated during the bituminous stage in the coalification process has escaped
143 from the coal source following basin uplift during Paleogene (Kotarba and Rice, 2001) and diffused through
144 fractures and faults occurring in tectonic zones. The late-stage gas generated by microbial reduction of CO₂ in the
145 coal seams at the top of the Carboniferous sequence accumulated under clay deposition in the Miocene (Kędzior,
146 2009).

147 2.1.3 Australia: Hunter Coalfield (Sydney Basin)

148 The Hunter Coalfield is part of the Sydney Basin, on the east coast of New South Wales in Australia, and consists
149 of 3 major coal measures. The deepest is the early Permian Greta Coal Measures, which is overlain by the late
150 Permian Whittingham Coal Measures and upper Newcastle Coal Measures. Throughout the Hunter coalfield all
151 sedimentary strata are gently folded, and the same coal seam can be mined at the ground surface and at depths of
152 several hundred meters. In the region surveyed both the opencast and underground mines are extracting coal from
153 the Whittingham coal measures, which are generally high volatile bituminous coals, although some medium to
154 low bituminous coals are extracted (Ward and Kelly, 2013). The mining operation is on a much larger scale than

155 in the UK - the total coal production for the Hunter Coalfield was 123.63 Mt in 2011, of which 88.24 Mt was
156 saleable (State of New South Wales, 2013) - and methane emissions are estimated to contribute 4.6% to global
157 coal-derived methane (US EPA, 2012). Several studies have attested to the dispersion of thermogenic methane
158 formed at higher degrees of coalification (i.e. high temperatures and pressures) during the uplift and the
159 subsequent erosion of the basin, followed by the replenishment of the unsaturated basin with more recently formed
160 methane of biogenic origin (Faiz and Hendry, 2006; Burra, 2010). Gas emplacement is related to sorption capacity
161 of coal strata, in particular to the pore pressure regime, which is influenced by the local geological features
162 (compressional or extensional) of the basin. The south of the Hunter Coalfield is characterised by higher gas
163 content and enhanced permeability than the northern area, with a large potential for methane production, mainly
164 biogenic (Pinetown, 2014).

165 **2.2 Sampling and measurement methodology**

166 For isotopic characterisation of the methane sources, integrated methane emissions were assessed through
167 detection of the offsite downwind plume. In fact, even when emissions are focused on defined locations, such as
168 vent pipes in underground mines, the methane provenance cannot be localised, since most of collieries are not
169 accessible. For sample collection and measurements of methane emissions downwind of coal mines in the UK
170 and Australia the mobile system described by Zazzeri et al. (2015) has been implemented. The system utilises a
171 Picarro G2301 CRDS (Cavity Ring-Down Spectroscopy) within the survey vehicle, for continuous CH₄ and CO₂
172 mole fraction measurements, and a mobile module including air inlet, sonic anemometer and GPS receiver on the
173 roof of the vehicle. The entire system is controlled by a laptop, which allows methane mole fractions and the
174 methane plume outline to be displayed in real time on a Google Earth platform during the survey to direct plume
175 sampling. When the plume was encountered, the vehicle was stopped and air samples collected in 3L Tedlar bags,
176 using a diaphragm pump connected to the air inlet. Samples were taken at different locations along the plume
177 transect in order to obtain a wide range of methane mole fractions and isotopic signatures in the collected air. The
178 Upper Silesian basin was surveyed with a Picarro 2101-i measuring continuous CO₂ and CH₄ mole fractions and
179 $\delta^{13}\text{C}\text{CO}_2$ isotopic ratio. Samples were collected on site for analysis of $\delta^{13}\text{C}\text{CH}_4$ isotopic ratio.

180 The carbon isotopic ratio ($\delta^{13}\text{C}\text{CH}_4$) of bag samples was measured in the greenhouse gas laboratory at RHUL
181 (Royal Holloway University of London) in triplicate to high precision (± 0.05 ‰) by continuous flow gas
182 chromatography isotope ratio mass spectrometry (CF GC-IRMS) (Fisher et al., 2006). CH₄ and CO₂ mole fractions
183 of samples were measured independently in the laboratory with a Picarro G1301 CRDS analyser, calibrated
184 against the NOAA (National Oceanic and Atmospheric Administration) WMO-2004A and WMO-X2007
185 reference scales respectively. The $\delta^{13}\text{C}\text{CH}_4$ signature for each emission plume was calculated using the Keeling
186 plot approach, according to which the $\delta^{13}\text{C}$ isotopic composition of samples and the inverse of the relative mole
187 fractions have a linear relationship, whose intercept represents the isotopic signature of the source (Pataki et al.,
188 2003). Source signatures were provided with the relative uncertainty, computed by the BCES (Bivariate
189 Correlated Errors and intrinsic Scatter) estimator (Akritas and Bershadsky, 1996), which accounts for correlated
190 errors between two variables and calculates the error on the slope and intercept of the best interpolation line. Mole
191 fraction data and co-located coordinates were used to map the mole fraction variability using the ArcGIS software.

192 3 Results and Discussion

193 While most of the emissions from deep mines come specifically from ventilation shafts, which are point sources,
194 emissions from open-cut mines are wide-spread, and difficult to estimate. However, the objective of this study is
195 not the quantification of emissions, but the assessment of the overall signature of methane released into the
196 atmosphere, made through the sampling of integrated emissions from the whole area. Therefore, even though
197 onsite access to collieries was not possible, by driving around the contiguous area, methane emissions could be
198 intercepted and their mole fractions measured. Table 1 summarises $\delta^{13}\text{CCH}_4$ signatures of all the coal mines and
199 coal basins surveyed with the Picarro mobile system.

200 3.1 English coal mines

201 Methane plumes from Hatfield colliery, one of the few UK deep mines still open at the time of this study, were
202 detected during surveys on 10th July and 26th September 2013. The methane desorbed from coal heaps within the
203 colliery area and methane vented from shafts might explain the relatively high mole fractions measured (up to 7
204 ppm). Keeling plots based on the samples collected (4 on the first and 5 on the second survey) give intercept
205 values of -48.3 ± 0.2 and -48.8 ± 0.3 ‰ (2SD).

206 Maltby colliery is one of the largest and deepest mines in England and was closed in March 2013. The coal mine
207 methane was extracted and used for electricity, but over 3 ppm mole fractions were detected in ambient air during
208 both surveys in July and September 2013, giving evidence of methane releases from the recovery system and
209 ventilation shafts. The Keeling plot intercepts based on the samples collected in July and in September are -45.9
210 ± 0.3 and -45.4 ± 0.2 ‰ (2SD) respectively, ~ 3 ‰ heavier than the isotopic source signatures calculated for Hatfield
211 Colliery on the same sampling days. Both source signatures are in good agreement with the value of -44.1 ‰
212 observed for desorbed methane of the Barnsley coal seam, in a study conducted by Hitchman et al. (1990b).

213 Kellingley colliery is a still open deep mine situated in North Yorkshire. A surface drainage plant for electrical
214 power generation has been implemented (Holloway et al., 2005), and methane releases from the power plant might
215 justify the mole fractions peak of 9 ppm that was observed while driving on the north side of the coal mine on 10th
216 July 2013. The Keeling plot analysis of the samples collected indicates a source signature of -46.5 ± 0.3 ‰ (2SD).
217 The highest mole fractions detected around Thoresby mine, in Nottinghamshire, approached 5 ppm. Nine samples
218 were collected, giving a source signature of -51.2 ± 0.3 ‰ (2SD).

219 During the sampling of methane plumes from Daw Mill colliery, the highest methane mole fractions (~ 5 ppm)
220 were recorded close to the edge of the colliery, whereas, driving downwind of the site at further distances, only
221 background values were measured. Indeed, the estimated methane content of the coal seam exploited in Daw Mill
222 colliery, closed in March 2013, is low (typically about $1.7 \text{ m}^3/\text{tonne}$) and, furthermore, a ventilation system is
223 implemented, so that the coal mine methane potential is curtailed (Drake, 1983). Keeling plot analysis reveals a
224 source signature of -51.4 ± 0.2 ‰ (2SD).

225 3.2 Welsh coal mines

226 Methane emissions from coal mines in Wales were sampled in order to characterise methane releases from a
227 different rank of coal. The area investigated extended from Cwmllynfell to Merthyr Tydfil. The South Wales
228 coalfield is estimated to have the highest measured seam gas content in the UK (Creedy, 1991).

229 **3.2.1 Deep Mines**

230 The deep mine Aberpergwm, which closed in December 2012, did not operate coal mine methane schemes and
231 methane was vented up to the surface as part of standard operation systems (Holloway et al., 2005). That is
232 consistent with methane mole fractions peaks of 6 ppm observed when approaching the colliery. Air samples were
233 also collected near Unity deep mine, Wales' largest drift mine, which reopened in 2007 and is located in the town
234 of Cwmgwrach, only 1.5 km away from Aberpergwm. Isotopic source signatures of $-33.3 \pm 1.8 \text{ ‰}$ and -30.9 ± 1.4
235 ‰ result from the Keeling plots based on samples collected respectively near Aberpergwm and Unity colliery,
236 both highly ^{13}C enriched relative to all English collieries.

237 **3.2.2 Opencast Mines**

238 The Picarro mobile system was driven around opencast mines at Cwmllynfell and Abercrave, in the Swansea
239 Valley. Up to 3 ppm methane mole fractions were recorded near the two mines, which were closed in the 1960s
240 as drift mines and are currently exploited as opencast mines. Our measurements confirm that they are still emitting
241 methane, even though the methane mole fractions recorded downwind of the mines were not significantly above
242 background. ^{13}C signatures between -41.4 ± 0.5 and $-41.2 \pm 0.9 \text{ ‰}$ (2SD) result from isotopic analysis of samples
243 collected downwind of the opencast mines, approximately 10 ‰ lower than the isotopic signature characterising
244 Welsh deep anthracite mines.

245 **3.3 Polish coal mine**

246 A Picarro mobile survey of the Upper Silesian basin took place on 10th June 2013 and 12 air samples were
247 collected for isotopic analysis. All the mines in this area are deep mines, exploiting the coal at depths ranging
248 from 300 to 900 m. The Keeling plot analysis includes 8 samples collected around the area of Radoszowy,
249 downwind of the KWK Wujek deep mine shafts. Methane mole fractions in the range of 3-5 ppm were measured
250 in the majority of the area of Katowice and over 20 ppm mole fractions were detected when transecting the plume
251 originating from the exhaust shafts, which confirms the high level of methane that the mine contains. A source
252 signature of $-50.9 \pm 0.6 \text{ ‰}$ (2SD) was calculated by Keeling plot analysis, which is consistent with the values
253 obtained for the deep mined English bituminous coal.

254 **3.4 Australia: Hunter Coalfield**

255 On 12th and 18th March 2014 12 samples in total were collected along the route in the Hunter Coalfield, where the
256 bituminous coal strata of the Sydney Basin are extracted both in opencast and underground mines. The methane
257 plume width was in the range of 70 km (Fig. 1). A maximum mole fraction of 13.5 ppm was measured near a vent
258 shaft associated with the Ravensworth underground mine (see white star in Fig. 1b). The source signature
259 calculated by the Keeling plot analysis based on all the samples collected during both surveys (grey markers in
260 Fig. 2c) is $-66.4 \pm 1.3 \text{ ‰}$ (2SD) and this signature likely includes a mixture of methane derived both from
261 underground and opencast mines. Two samples collected downwind of the Ravensworth ventilation shaft (red
262 pushpins in Fig. 1b) fall off the Keeling plot trend for March 2014 and are not included in the calculation, because
263 they are likely dominated by methane from the vent shaft and are not representative of the regional mixed isotopic
264 signature.

265 In January 2016, 10 samples were collected downwind of a ventilation fan in the Bulga mine (second white star
266 in Fig. 1b). The Keeling plot for these (black circles in Fig. 2c) indicates a $\delta^{13}\text{C}$ source signature of $-60.8 \pm 0.3 \text{ ‰}$
267 (2SD). The samples collected next to the Ravensworth ventilation shaft in 2014 fit on this Keeling plot, suggesting
268 that the $\delta^{13}\text{CCH}_4$ isotopic signature of emissions from underground works in the Hunter Coalfield is consistent.

269 **3.5 New representative $\delta^{13}\text{CCH}_4$ isotopic signatures for coal-derived methane**

270 The $\delta^{13}\text{CCH}_4$ isotopic values for coal have been found to be characteristic of single basins, but general assumptions
271 can be made to characterise coal mines worldwide. Table 2 provides the literature $\delta^{13}\text{CCH}_4$ isotopic values
272 characteristic of specific coal basins. The isotopic signatures of emissions from English bituminous coal are
273 consistent with the range of -49 to -31 ‰ suggested by Colombo et al. (1970) for in situ coal bed methane in the
274 Ruhr basin in Germany, which contains the most important German bituminous coal of Upper Carboniferous age
275 and low volatile anthracite (Thomas, 2002). Progression in coal rank might explain the value of -50 ‰ for
276 emissions from English underground mined bituminous coal and -30 ‰ for anthracite deep mines, followed by a
277 $5\text{-}10 \text{ ‰}$ ^{13}C -depletion likely caused by the incursion of meteoric water in the basin and the subsequent production
278 of secondary biogenic methane (Scott et al., 1994), resulting in -40 ‰ for methane plumes from Welsh open-cut
279 anthracite mines.

280 The link between coal rank and $\delta^{13}\text{CCH}_4$ isotopic signature is appreciable in the study of UK coal mines, but
281 differences in the $^{13}\text{C}/^{12}\text{C}$ isotopic ratio within the same coal sequences could be ascribed to other parameters,
282 such as the depth at which the coal is mined - as methane migrates towards the surface, diffusion or microbial
283 fractionation may occur, especially if there is water ingress (see section 1). In particular, emissions from Thoresby
284 are more ^{13}C depleted than those measured around Maltby, although both mines exploit the Parkgate seam (see
285 Table 1), meaning that different isotopic signatures cannot be entirely linked to the coal rank. Biogenic methane
286 produced in a later stage due to water intrusion might have been mixed with the original thermogenic methane
287 formed during the coalification process.

288 Differences in methane emissions and their isotopic signature between opencast and deep mines have been
289 assessed by surveying both surface and underground mines, in the Welsh anthracite belt, and in the Hunter
290 Coalfield. The shallower deposits are more exposed to the weathering and meteoric water, most likely associated
291 with the production of some isotopically lighter microbial methane. Mole fractions up to 2.5 ppm were measured
292 around opencast mines in the Hunter Coalfield, in Australia, within a methane plume of more than 70 km width.
293 The highest methane mole fractions were consistently measured downwind of vent shafts in underground mines.
294 The difference in the source isotopic signature for methane emissions between the two types of mining both in
295 the Hunter Coalfield (from -61 to -66 ‰) and in Wales (from -31 to -41 ‰) reflects the isotopic shift of $5\text{-}10 \text{ ‰}$
296 that might be attributed to the occurrence of secondary biogenic methane.

297 The $\delta^{13}\text{C}$ signatures for coalbed methane emissions from the Upper Silesian basin are highly variable, with the
298 most ^{13}C depleted methane associated with diffusion processes or secondary microbial methane generation
299 (Kotarba and Rice, 2001), but the value of -51 ‰ measured for methane emissions from the KWK Wujek deep
300 mine is consistent with the value of -50 ‰ inferred for emissions from English bituminous coal extracted in
301 underground mines.

302 Figure 3 shows the $\delta^{13}\text{CCH}_4$ signatures ranges for each coal type, based on the results of this study and isotopic
303 values found in literature.

304 **4 Conclusions**

305 By measuring the isotopic signatures of methane plumes from a representative spread of coal types and depths,
306 we show that the $\delta^{13}\text{C}$ isotopic value to be included in regional and global atmospheric models for the estimate of
307 methane emissions from the coal sector must be chosen according to coal rank and type of mining (opencast or
308 underground). For low resolution methane modelling studies, our measurements suggest an averaged value of -
309 65 ‰ for bituminous coal exploited in open cast mines and of -55 ‰ or less negative, in deep mines, whereas
310 values of -40 ‰ and -30 ‰ can be assigned to anthracite opencast and deep mines respectively. However, the
311 ranges of isotopic signatures of methane emitted from each of these categories are wide (see Fig. 3), and the
312 isotopic ratios of methane from Chinese coal mines is little studied. Further measurements would be required in
313 other coal mining areas, especially China, to determine appropriate values for global modelling of methane
314 isotopes.

315 Global methane budget models that incorporate isotopes have used a $\delta^{13}\text{C}$ signature of -35 ‰ for coal or a value
316 -40 ‰ for total fossil fuels (e.g. Hein et al., 1997; Mikaloff Fletcher et al., 2004; Bousquet et al., 2006; Monteil
317 et al., 2011), but, given the relative rarity of anthracite global coal reserves and the dominance of bituminous coal
318 (1% and 53% respectively) (World Coal Institute, 2015), it seems likely that a global average emission from coal
319 mining activities will be lighter, with the -50 ‰ recorded for deep-mined bituminous coal in Europe being a closer
320 estimate. However, for detailed global modelling of atmospheric methane, isotopic signatures of coal emissions
321 should be region or nation specific, as greater detail is needed given the wide global variation. The assignment of
322 an incorrect global mean, or a correct global mean but inappropriate for regional scale modelling, might lead to
323 incorrect emissions estimates or source apportionment. The new scheme gives the possibility for an educated
324 estimate of the $\delta^{13}\text{C}$ signature of emission to atmosphere to be made for an individual coal basin or nation, given
325 information on the type of coal being mined and the method of extraction.

326 In conclusion, high-precision measurements of $\delta^{13}\text{C}$ in plumes of methane emitted to atmosphere from a range of
327 coal mining activities have been used to constrain the isotopic range for specific ranks of coal and mine type,
328 offering more representative isotopic signatures for use in methane budget assessment at regional and global
329 scales.

330 **Acknowledgements**

331 Giulia Zazzeri would like to thank Royal Holloway, University of London for provision of a Crossland scholarship
332 and a contribution from the Department of Earth Sciences from 2011 to 2014. Analysis of samples from Poland
333 was funded through the European Community's Seventh Framework Programme (FP7/2007-2013) in the InGOS
334 project under grant agreement n. 284274. Sampling in Australia was possible due to a grant from the Cotton
335 Research and Development Corporation.

336 **References**

337 Akritas, M.G., and Bershady, M.A., 1996, Linear regression for astronomical data with measurement errors and
338 intrinsic scatter: *Astrophysical Journal*, v. 470, p. 706-714.

339 Alderton, D., Oxtoby, N., Brice, H., Grassineau, N., and Bevins, R., 2004, The link between fluids and rank
340 variation in the South Wales Coalfield: evidence from fluid inclusions and stable isotopes: *Geofluids*, v. 4,
341 p. 221-236.

342 Aravena, R., Harrison, S., Barker, J., Abercrombie, H., and Rudolph, D., 2003, Origin of methane in the Elk
343 Valley coalfield, southeastern British Columbia, Canada: *Chemical Geology*, v. 195, p. 219-227.

344 Bates, B.L., McIntosh, J.C., Lohse, K.A., and Brooks, P.D., 2011, Influence of groundwater flowpaths, residence
345 times and nutrients on the extent of microbial methanogenesis in coal beds: Powder River Basin, USA:
346 *Chemical Geology*, v. 284, p. 45-61.

347 Bousquet, P., Ciais, P., Miller, J., Dlugokencky, E., Hauglustaine, D., Prigent, C., Van der Werf, G., Peylin, P.,
348 Brunke, E.-G., and Carouge, C., 2006, Contribution of anthropogenic and natural sources to atmospheric
349 methane variability: *Nature*, v. 443, p. 439-443.

350 Bulga Underground Operations Mining: Operation Plan 2015 to 2021, 2015.

351 Burra, A., 2010, Application of domains in gas-in-place estimation for opencut coal mine fugitive gas emissions
352 reporting, Bowen Basin Symposium, p. 59-64.

353 Chung, H.M., and Sackett, W.M., 1979, Use of stable carbon isotope compositions of pyrolytically derived
354 methane as maturity indices for carbonaceous materials: *Geochimica et Cosmochimica Acta*, v. 43, no.12.

355 Clayton, J., 1998, Geochemistry of coalbed gas—A review: *International Journal of Coal Geology*, v. 35, p. 159-
356 173.

357 Colombo U., G.F., Gonfiantini F., Gonfiantini R., Kneuper G., Teichmuller I., Teichmuller R. , 1970, Carbon
358 isotope study on methane from German coal deposits.: *Advances in Organic Geochemistry 1966* (eds G. D.
359 HOBSON and G. C. SPEERS), p. 1-26.

360 Creedy, D.P., 1991, An introduction to geological aspects of methane occurrence and control in British deep coal
361 mines: *Quarterly Journal of Engineering Geology*, v. 24, p. 209-220.

362 Dai, J.X., Qi, H.F., Song, Y., and Guan, D.S., 1987, Composition, carbon isotope characteristics and the origin of
363 coal-bed gases in China and their implication: *Scientia Sinica Series B-Chemical Biological Agricultural
364 Medical & Earth Sciences*, v. 30, p. 1324-1337.

365 Dai, J., Ni, Y., and Zou, C., 2012, Stable carbon and hydrogen isotopes of natural gases sourced from the Xujiahe
366 Formation in the Sichuan Basin, China: *Organic Geochemistry*, v. 43, p. 103-111.

367 Deines, P., 1980, The isotopic composition of reduced organic carbon: *Handbook of environmental isotope
368 geochemistry*, p. 329-406.

369 Drake, D., 1983, *Working the Warwickshire Thick Coal, Improved Techniques for the Extraction of Primary
370 Forms of Energy*, Springer Netherlands, p. 156-156.

371 Faiz, M., and Hendry, P., 2006, Significance of microbial activity in Australian coal bed methane reservoirs—a
372 review: *Bulletin of Canadian Petroleum Geology*, v. 54, p. 261-272.

373 Fisher, R., Lowry, D., Wilkin, O., Sriskantharajah, S., and Nisbet, E.G., 2006, High-precision, automated stable
374 isotope analysis of atmospheric methane and carbon dioxide using continuous-flow isotope-ratio mass
375 spectrometry: *Rapid Communications in Mass Spectrometry*, v. 20, p. 200-208.

376 Flores, R.M., Rice, C.A., Stricker, G.D., Warden, A., and Ellis, M.S., 2008, Methanogenic pathways of coal-bed
377 gas in the Powder River Basin, United States: the geologic factor: *International Journal of Coal Geology*, v.
378 76, p. 52-75.

379 Frodsham, K., and Gayer, R., 1999, The impact of tectonic deformation upon coal seams in the South Wales
380 coalfield, UK: *International Journal of Coal Geology*, v. 38, p. 297-332.

381 Fuex, A., 1980, Experimental evidence against an appreciable isotopic fractionation of methane during migration:
382 *Physics and Chemistry of the Earth*, v. 12, p. 725-732.

383 Fung, I., John, J., Lerner, J., Matthews, E., Prather, M., Steele, L., and Fraser, P., 1991, Three-dimensional model
384 synthesis of the global methane cycle: *Journal of Geophysical Research*, v. 96, no.D7.

385 GSS Environmental, 2012, Ravensworth Underground Mine: Liddell Seam Project.

386 Guo, H., Yu, Z., Liu, R., Zhang, H., Zhong, Q., and Xiong, Z., 2012, Methylophilic methanogenesis governs the
387 biogenic coal bed methane formation in Eastern Ordos Basin, China: *Applied microbiology and
388 biotechnology*, v. 96, p. 1587-1597.

389 Hein, R., Crutzen, P.J., and Heimann, M., 1997, An inverse modeling approach to investigate the global
390 atmospheric methane cycle: *Global Biogeochemical Cycles*, v. 11, p. 43-76.

391 Hill, A., 2001, *The South Yorkshire Coalfield: A History and Development*, Tempus Books, Gloucestershire.

392 Hitchman, S., Darling, W., and Williams, G., 1990a, Stable isotope ratios in methane containing gases in the
393 United Kingdom.

394 Hitchman, S., Darling, W., and Williams, G., 1990b, Stable isotope ratios in methane containing gases in the
395 United Kingdom. Report of the British Geological Survey, Processes Research Group WE/89/30.

396 Holloway, S., Jones, N., Creedy, D., and Garner, K., 2005, Can new technologies be used to exploit the coal
397 resources in the Yorkshire-Nottinghamshire coalfield?: *Carboniferous Hydrocarbon Geology: The Southern
398 North Sea Surrounding Areas*, v. 7 Occasional publications of the Yorkshire Geological Society, p. 195–
399 208.

400 IMC Group Consulting Limited, 2002, A review of the remaining reserves at deep mines for the Department of
401 Trade and Industry.

402 IPCC, 2006, 2006 IPCC guidelines for national greenhouse gas inventories: industrial processes and product use,
403 Kanagawa, JP: Institute for Global Environmental Strategies.

404 Jureczka, J., and Kotas, A., 1995, Coal deposits—Upper Silesian Coal Basin: The carboniferous system in Poland,
405 v. 148, p. 164-173.

406 Kanduč, T., Grassa, F., Lazar, J., and Zavšek, S., 2015, Geochemical and isotopic characterization of coalbed
407 gases in active excavation fields at Preloge and Pesje (Velenje Basin) mining areas: *RMZ–M&G*, v. 62, p.
408 21-36.

409 Kędzior, S., 2009, Accumulation of coal-bed methane in the south-west part of the Upper Silesian Coal Basin
410 (southern Poland): *International Journal of Coal Geology*, v. 80, p. 20-34.

411 Kotarba, M.J., and Rice, D.D., 2001, Composition and origin of coalbed gases in the Lower Silesian basin,
412 southwest Poland: *Applied Geochemistry*, v. 16, p. 895-910.

413 Kinnon, E., Golding, S., Boreham, C., Baublys, K., and Esterle, J., 2010, Stable isotope and water quality analysis
414 of coal bed methane production waters and gases from the Bowen Basin, Australia: *International Journal of
415 Coal Geology*, v. 82, p. 219-231.

416 Levin, I., Bergamaschi, P., Dörr, H., and Trapp, D., 1993, Stable isotopic signature of methane from major sources
417 in Germany: *Chemosphere*, v. 26, p. 161-177.

418 Liptay, K., Chanton, J., Czepiel, P., and Mosher, B., 1998, Use of stable isotopes to determine methane oxidation
419 in landfill cover soils: *Journal of Geophysical Research: Atmospheres* (1984–2012), v. 103, p. 8243-8250.

420 Locatelli, R., Bousquet, P., Chevallier, F., Fortems-Cheney, A., Szopa, S., Saunois, M., Agusti-Panareda, A.,
421 Bergmann, D., Bian, H., and Cameron-Smith, P., 2013, Impact of transport model errors on the global and
422 regional methane emissions estimated by inverse modelling: *Atmospheric chemistry and physics*, v. 13, p.
423 9917-9937.

424 Lowry, D., Holmes, C.W., Rata, N.D., O'Brien, P., and Nisbet, E.G., 2001, London methane emissions: Use of
425 diurnal changes in concentration and $\delta^{13}\text{C}$ to identify urban sources and verify inventories: *Journal of*
426 *Geophysical Research: Atmospheres*, v. 106, p. 7427-7448.

427 McEvoy F. M., M.D., Harrison D.J., Cameron D.G., Burke H.F., Spencer N.A., Evans D.J., Lott G.K., Hobbs S.F.
428 and Highley D.E., 2006, Mineral Resource Information in Support of National, Regional and Local Planning:
429 South Yorkshire (comprising Metropolitan Boroughs of Barnsley, Doncaster and Rotherham and City of
430 Sheffield) British Geological Survey Commissioned Report.

431 Maher, D.T., Santos, I.R., and Tait, D.R., 2014, Mapping methane and carbon dioxide concentrations and $\delta^{13}\text{C}$
432 values in the atmosphere of two Australian coal seam gas fields: *Water, Air, & Soil Pollution*, v. 225, p. 1-
433 9.

434 Martini, A., Walter, L., Budai, J., Ku, T., Kaiser, C., and Schoell, M., 1998, Genetic and temporal relations
435 between formation waters and biogenic methane: Upper Devonian Antrim Shale, Michigan Basin, USA:
436 *Geochimica et Cosmochimica Acta*, v. 62, p. 1699-1720.

437 Mikaloff Fletcher, S.E., Tans, P.P., Bruhwiler, L.M., Miller, J.B., and Heimann, M., 2004, CH₄ sources estimated
438 from atmospheric observations of CH₄ and its $^{13}\text{C}/^{12}\text{C}$ isotopic ratios: 2. Inverse modeling of CH₄ fluxes
439 from geographical regions: *Global Biogeochemical Cycles*, v. 18, no.4.

440 Miller, J.B., 2004, The carbon isotopic composition of atmospheric methane and its constraints on the global
441 methane budget, *Stable Isotopes and Biosphere-Atmosphere Interactions: Processes and Biological Controls*,
442 Elsevier Academic Press California, p. 288-306.

443 Monteil, G., Houweling, S., Dlugokenky, E., Maenhout, G., Vaughn, B., White, J., and Rockmann, T., 2011,
444 Interpreting methane variations in the past two decades using measurements of CH₄ mixing ratio and isotopic
445 composition: *Atmospheric chemistry and physics*, v. 11, p. 9141-9153.

446 Nisbet, E.G., Dlugokenky, E.J., and Bousquet, P., 2014, Methane on the rise—again: *Science*, v. 343, p. 493-
447 495.

448 O'Keefe, J.M., Bechtel, A., Christanis, K., Dai, S., DiMichele, W.A., Eble, C.F., Esterle, J.S., Mastalerz, M.,
449 Raymond, A.L., and Valentim, B.V., 2013, On the fundamental difference between coal rank and coal type:
450 *International Journal of Coal Geology*, v. 118, p. 58-87.

451 Papendick, S.L., Downs, K.R., Vo, K.D., Hamilton, S.K., Dawson, G.K., Golding, S.D., and Gilcrease, P.C., 2011,
452 Biogenic methane potential for Surat Basin, Queensland coal seams: *International Journal of Coal Geology*,
453 v. 88, p. 123-134.

454 Pataki, D.E., Bowling, D.R., and Ehleringer, J.R., 2003, Seasonal cycle of carbon dioxide and its isotopic
455 composition in an urban atmosphere: Anthropogenic and biogenic effects: *Journal of Geophysical Research-*
456 *Atmospheres*, v. 108, no.D23.

457 Patyńska, R., 2013, Prognoza wskaźników emisji metanu z kopalń metanowych węgla kamiennego w Polsce:
458 Polityka Energetyczna, v. 16.

459 Pinetown, K., 2014, Regional coal seam gas distribution and burial history of the Hunter Coalfield, Sydney Basin:
460 Australian Journal of Earth Sciences, v. 61, p. 409-426.

461 Qin, S., Tang, X., Song, Y., and Wang, H., 2006, Distribution and fractionation mechanism of stable carbon
462 isotope of coalbed methane: Science in China Series D: Earth Sciences, v. 49, p. 1252-1258.

463 Rice, D.D., 1993, Composition and origins of coalbed gas: Hydrocarbons from coal: AAPG Studies in Geology,
464 v. 38, p. 159-184.

465 Rice, D.D., Clayton, J.L., and Pawlewicz, M.J., 1989, Characterization of coal-derived hydrocarbons and source-
466 rock potential of coal beds, San Juan Basin, New Mexico and Colorado, USA: International Journal of Coal
467 Geology, v. 13, p. 597-626.

468 Scott, A.R., 2002, Hydrogeologic factors affecting gas content distribution in coal beds: International Journal of
469 Coal Geology, v. 50, p. 363-387.

470 Scott, A.R., Kaiser, W., and Ayers Jr, W.B., 1994, Thermogenic and secondary biogenic gases, San Juan Basin,
471 Colorado and New Mexico--implications for coalbed gas producibility: AAPG bulletin, v. 78, p. 1186-1209.

472 Smith, J.W., Gould, K., and Rigby, D., 1981, The stable isotope geochemistry of Australian coals: Organic
473 Geochemistry, v. 3, p. 111-131.

474 Stach, E., and Murchison, D.G., 1982, Stach's Textbook of coal petrology, Borntraeger, Stuttgart (1982), 426 p.
475 State of New South Wales, Department of Trade & Investment, Division of Resources & Energy (2013). 2013
476 New South Wales Coal Industry profile.

477 Strapóć, D., Mastalerz, M., Eble, C., and Schimmelmann, A., 2007, Characterization of the origin of coalbed gases
478 in southeastern Illinois Basin by compound-specific carbon and hydrogen stable isotope ratios: Organic
479 Geochemistry, v. 38, p. 267-287.

480 Su, X., Lin, X., Liu, S., Zhao, M., and Song, Y., 2005, Geology of coalbed methane reservoirs in the Southeast
481 Qinshui Basin of China: International Journal of Coal Geology, v. 62, p. 197-210.

482 Thomas, L., 2002, Coal geology, John Wiley & Sons.

483 Townsend-Small, A., Tyler, S.C., Pataki, D.E., Xu, X.M., and Christensen, L.E., 2012, Isotopic measurements of
484 atmospheric methane in Los Angeles, California, USA: Influence of "fugitive" fossil fuel emissions: Journal
485 of Geophysical Research-Atmospheres, v. 117, no.D7.

486 U.S. EPA, 2012, Global Anthropogenic Non-CO₂ Greenhouse Gas Emissions: 1990- 030, USEPA, Washington,
487 DC, EPA 430-R-12-006

488 U.S. EPA, 2013, US Environmental Protection Agency, Global Mitigation of Non-CO₂ Greenhouse Gases: 2010–
489 2030, USEPA, Washington, DC, EPA-430-R-13-011.

490 Waldron, S., Fallick, A., and Hall, A., 1998, Comment on" Spatial distribution of microbial methane production
491 pathways in temperate zone wetland soils: Stable carbon and hydrogen evidence" by ERC Hornibrook, FJ
492 Longstaffe, and WS Fyfe: Geochimica et Cosmochimica Acta, v. 62, p. 369-372.

493 Ward, C., and Kelly, B.F.J., 2013, Background Paper on New South Wales Geology: with a focus on basins
494 containing coal seam gas resources., UNSW Global, The University of New South Wales, a report prepared
495 for the Office of the NSW Chief Scientist and Engineer.

496 Whiticar, M., and Schaefer, H., 2007, Constraining past global tropospheric methane budgets with carbon and
497 hydrogen isotope ratios in ice: *Philosophical Transactions of the Royal Society of London A: Mathematical,*
498 *Physical and Engineering Sciences*, v. 365, p. 1793-1828.

499 Whiticar, M.J., 1996, Stable isotope geochemistry of coals, humic kerogens and related natural gases:
500 *International Journal of Coal Geology*, v. 32, p. 191-215.

501 Whiticar, M.J., 1999, Carbon and hydrogen isotope systematics of bacterial formation and oxidation of methane:
502 *Chemical Geology*, v. 161, p. 291-314.

503 World Coal Institute, 2015, The coal resource, a comprehensive overview of coal: <http://www.worldcoal.org/>

504 Xiong, Y., Geng, A., and Liu, J., 2004, Kinetic-simulating experiment combined with GC-IRMS analysis:
505 application to identification and assessment of coal-derived methane from Zhongba Gas Field (Sichuan
506 Basin, China): *Chemical Geology*, v. 213, p. 325-338.

507 Yao, Y., D. Liu and Y. Qiu, 2013, Variable gas content, saturation, and accumulation characteristics of Weibei
508 coalbed methane pilot-production field in the southeastern Ordos Basin, China: *AAPG bulletin*, v. 97, p.
509 1371-1393.

510 Zazzeri, G., Lowry, D., Fisher, R., France, J., Lanoisellé, M., and Nisbet, E., 2015, Plume mapping and isotopic
511 characterisation of anthropogenic methane sources: *Atmospheric Environment*, v. 110, p. 151-162.

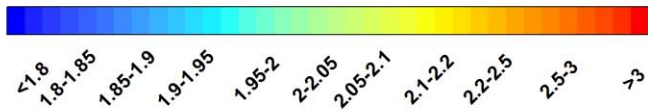
Sampling Site	Country	Coal seam	Coal Type	Mine Type	Sampling Date	$\delta^{13}\text{C}$ Signatures [‰]	Samples used in Keeling plots	number
Kellingley Colliery (active)	North Yorkshire/UK	Beeston and Silkstone coal seams	Bituminous coal	Deep Mine	Sept-2013	-46.5 ±0.3	5	
Maltby Colliery (closed since March 2013)	South Yorkshire/UK	Barnsley and Parkgate seams, up to 991 m in depth (McEvoy et al., 2006)	Bituminous coal	Deep Mine	Jul-2013	-45.9 ±0.3	3	
					Sept-2013	-45.4 ±0.2	4	
Hatfield Colliery (active)	South Yorkshire/UK	Barnsley (~401-465 m), Dunsil (414-376 m) High Hazel (~313-284 m) seams (Hill, 2001)	Bituminous coal	Deep Mine	Jul-2013	-48.3 ±0.2	4	
					Sept-2013	-48.8 ±0.3	5	
Thoresby Colliery (active)	Nottinghamshire/UK	Parkgate seam, ~650 m in depth	Bituminous coal	Deep Mine	Nov-2013	-51.2 ±0.3	9	
Daw Mill Colliery (closed since March 2013)	Warwickshire/UK	Warwickshire Thick seam, from 500 to 1000 m in depth.	Bituminous coal	Deep Mine	Nov-2013	-51.4 ±0.2	4	
Cwmllynfell Colliery (active)	Wales/UK	South Wales Coalfield*	Anthracite	Surface Mine	Oct-2013	-41.2 ±0.9	4	
Abercrave Colliery (active)	Wales/UK	South Wales Coalfield	Anthracite	Surface Mine	Oct-2013	-41.4 ±0.5	5	
Aberpergwm Colliery (closed since December 2012)	Wales/UK	South Wales Coalfield	Anthracite	Deep Mine	Oct-2013	-33.3 ±1.8	5	
Unity Colliery (active)	Wales/UK	South Wales Coalfield	Anthracite	Deep Mine	Oct-2013	-30.9 ±1.4	3	
Hunter Coalfield (active)	Australia	Whittingham Coal Measures	Bituminous coal	Surface and Deep Mines	Mar-2014	-66.4 ±1.3	12	
Bulga Colliery (active)	Australia	Blakefield South Seam, from 130 to 510 m in depth (Bulga Underground Operation mining, 2015)	Bituminous coal	Deep Mine	Jan-2016	-60.8 ±0.3	10	
Upper Silesian Basin (active)	Poland	502 (590-634m) and 510 seam (763-812m)	Bituminous coal	Deep Mine	Jun-2013	-50.9 ± 1.2	8	

512 **Table 1 $\delta^{13}\text{CCH}_4$ signatures of all the coal mines and coal basins surveyed with the Picarro mobile system. Errors in the $\delta^{13}\text{C}$ signatures are calculated as 2 standard deviations. *Only**
513 **the coalfield is indicated, as the name of the seams exploited could not be retrieved.**

Site	Coal Rank	$\delta^{13}\text{C}$ (‰)	Author	$\delta^{13}\text{C}$ (‰) measured in this study
Powder River Basin, U.S.A	Sub-bituminous coal	-79.5 to -56.8	Bates et al. (2011)	
Australia	From brown coal to low volatile bituminous coal.	-73.0 to -43.5	Smith et al. (1981)	-66.4 \pm 1.3 to -55.5 \pm 1.3
Velenje Basin, Slovenia	Lignite	-71.8 to -43.4	Kanduč et al. (2015)	
Powder River Basin, U.S.A.	Sub-bituminous coal	-68.4 to -59.5	Flores et al. (2008)	
Illinois Basin, U.S.A.	Bituminous coal	-66.6 to -56.8	Strapoć et al. (2007)	
Elk Valley Coalfield, Canada	Bituminous coal	-65.4 to -51.8	Aravena et al. (2003)	
Bowen basin, Australia	Bituminous coal	-62.2 to -48	Kinnon et al. (2010)	
Queensland Basin, Australia	From Sub-bituminous to high volatile bituminous	-57.3 to -54.2	Papendick et al. (2011)	
Tara region, Queensland Basin, Australia	From Sub-bituminous to high volatile bituminous	-56.7	Maher et al. (2014)	
San Juan basin, New Mexico and Colorado	High-volatile Bituminous coal	-43.6 to -40.5	Rice et al. (1989)	
Michigan Basin, U.S.A.	Bituminous coal	-56 to -47	Martini et al. (1998)	
UK, Barnsley seam	Bituminous coal	-44.1	Hitchman et al. (a, b)	-48.8 \pm 0.3 to -45.4 \pm 0.2
Upper Silesian Coal Basin, Poland	Sub-bituminous coal to anthracite	-79.9 to -44.5	Kotarba and Rice (2001)	-50.9 \pm 0.6
Eastern China	Sub-bituminous to anthracite	-66.9 to -24.9	Dai et al. (1987)	
Ruhr basin, Germany	Bituminous coal, Anthracite	-37 (-60 to -14)	Deines (1980)	
Western Germany	High-volatile bituminous to anthracite.	-70.4 to -16.8	Colombo et al. (1970)	
Eastern Ordos Basin, China	Bituminous Coal	-42.3 to -39.8	Guo et al. (2012)	
South-eastern Ordos Basin, China	Low-volatile bituminous and semi-anthracite	-48.1 to -32.8	Yao et al. (2013)	
Qinshui, China	Anthracite	-41.4 to -34.0	Qin et al. (2006)	
Qinshui Basin, China	Semi-anthracite to Anthracite	-36.7 to -26.6	Su et al. (2005)	
Sichuan Basin, China	Bituminous to anthracite	-36.9 to -30.8	Dai et al. (2012)	
Wales, UK	Anthracite		Xiong et al. (2004)	-33.3 \pm 1.8 to -30.9 \pm 1.4

514 **Table 2 Literature isotope values obtained by methane samples CBM (Coalbed Methane) wells across the basin. Errors are not included in the sources.**

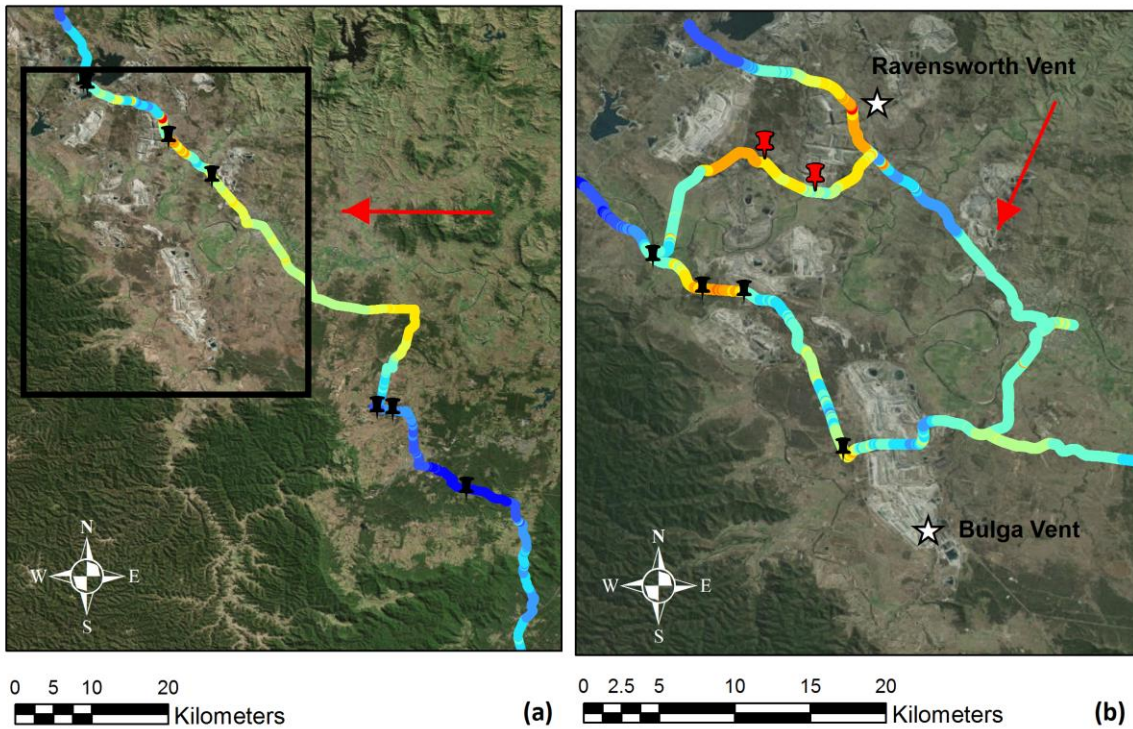
CH₄ Mole Fractions [ppm]



→ Wind Direction

📌 Samples collected in the Hunter Coalfield in March 2014

📌 Samples collected downwind of Ravensworth Vent



515

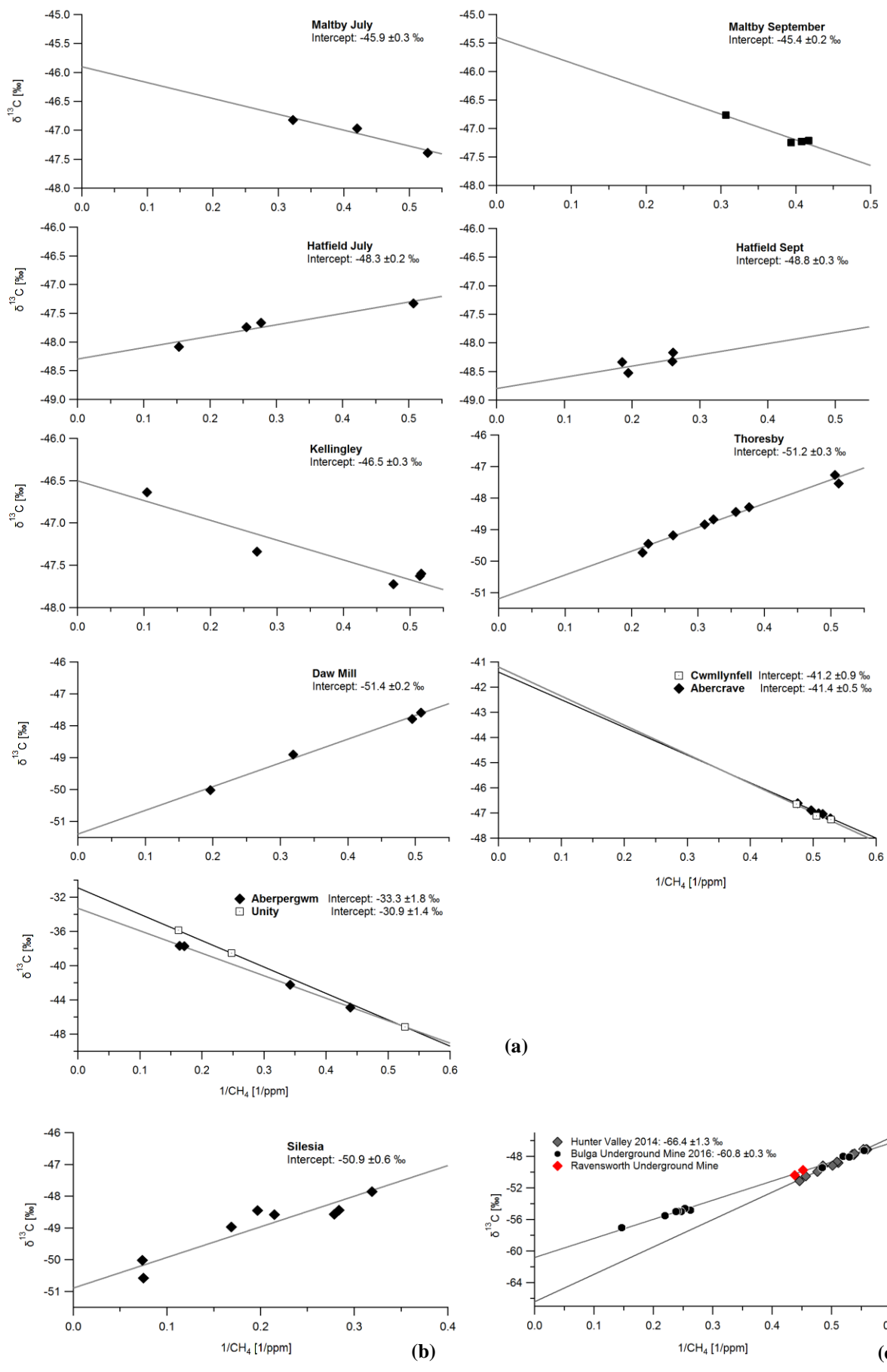
516

517

518

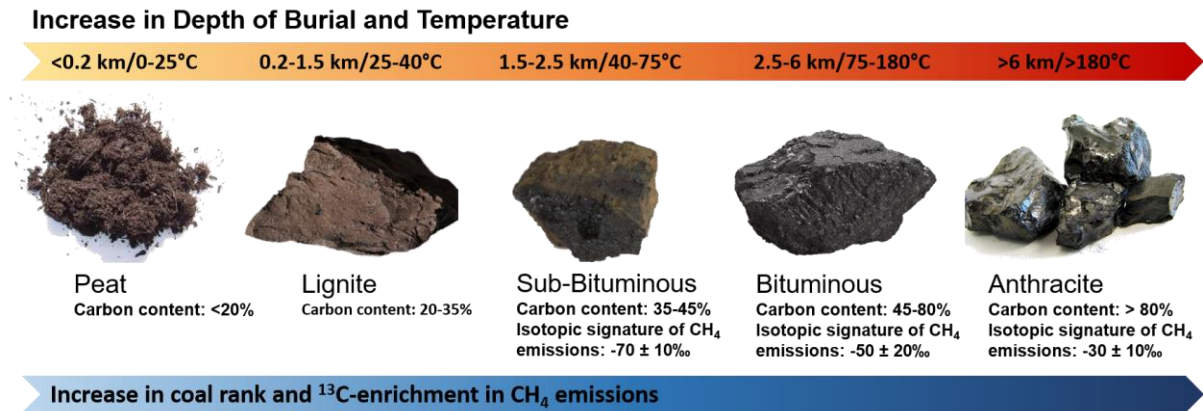
519

Figure 1 Methane mole fractions recorded in the Hunter Coalfield on 12th March 2014 (a) and during a more detailed survey of the area highlighted by the black square on 18th March 2014 (b). Source: Esri, DigitalGlobe, GeoEye, i-cubed, Earthstar Geographics, CNES/Airbus DS, USDA, USGS, AEX, Getmapping, Aerogrid, IGN, IGP, swisstopo and the GIS User Community.



520 Figure 2 Keeling Plots based on samples collected around English and Welsh coal mines (a), coal mines in Poland (b)
521 and Australia (c). Errors on the y-axis are within 0.05 ‰ and on the x-axis 0.0001 ppm⁻¹, and are not noticeable on the
522 graph.

523



524

525 Figure 3 Coal maturation process. The δ¹³CCH₄ signatures ranges are based on the literature values in Table 2 and on
526 the results of this study.

527

528

529